Available online at www.sciencedirect.com
SCIENCE DIRECT
Computers and Chemical Engineering 29 (2005) 2386–2403
Computers & Chemical Engineering
www.elsevier.com/locate/compchemeng

CFD analyses of complex flows

Richard Farmer [a,*], Ralph Pike [b], Gary Cheng [c]

[a] *University of Nevada Reno, ChE Department, UNR, Reno, NV 89557, USA*
[b] *ChE Department, LSU, Baton Rouge, LA, USA*
[c] *ME Department, UAB, Birmingham, AL, USA*

Received 11 May 2005; accepted 23 May 2005
Available online 2 September 2005

Abstract

Computational fluid dynamics (CFD) of complex processes and complicated geometries embraces the transport of momentum, heat, and mass including the description of reaction kinetics and thermodynamics. The paper outlines the numerical models available for analyzing these processes and presents examples of such methodology. The unprecedented growth in computer capability has resulted in efficient simulations of most transport phenomena. The aerospace's interest in high-pressure turbulent combustion has created efficient computational tools for analyzing run-away-reactions in the process industries. Practical turbulence models, generalized thermodynamic properties, and extensive chemical kinetics data bases are currently used in three-dimensional, steady-state simulations. However, industrial needs have challenged CFD modelers to improve their flow solvers in order to simulate flows with more complicated physics, such as spray combustion, acoustic waves, transient start-up and shut-down, and flow instabilities. In addition, the practicality and efficiency of numerical simulations are highly dependent on the submodels employed, such as reaction mechanisms and turbulence models. There has been some progress in generalizing CFD tools, but more development is needed. Most of all, more high-quality and critical test data are required to validate the CFD simulations of complex processes. The laminar transport equations have been averaged by various means to locally describe both turbulent and multi-phase flows. Spray combustion, stirred-tank reactors, fluidization of catalytic beds, and highly exothermic supercritical reactors are among the several validated examples, which illustrate today's technology. The designer's access to public-domain, open-source software offers powerful methodology for his use. Such software and the variety of available modeling techniques will be inventoried to demonstrate the scope of computational transport methodology. The current state of CFD models will be assessed to address the need for future research.

Keywords: Computational transport phenomenon; Process models; Model validation

1. Introduction

Today's computers offer unprecedented computational power to address complex chemical process operational and design issues. However, the practicing engineer's expertise in using this methodology and the availability of more demanding experimental validation data are required to reap the benefit of such simulation methodology. The partial differential equations, which represent turbulent flow and heat transfer were available over a hundred years before practical solution techniques were developed. Still, most process analyses are made with simplistic methods, especially with respect to the treatment of geometric flow variation. This paper outlines the various detailed modeling methods which are in use, and attempts to emphasize their similarities, in order to illustrate the analytical power which is currently within our reach. Specific examples will be presented to show what is possible, if we can effectively separate basic research studies from practical engineering approaches.

* Corresponding author. Tel.: +1 775 883 2417.
E-mail addresses: farmer@sierraengineering.com (R. Farmer), pike@she.lsu.edu (R. Pike), gcheng@uab.edu (G. Cheng).

0098-1354/$ – see front matter © 2005 Elsevier Ltd. All rights reserved.
doi:10.1016/j.compchemeng.2005.05.022

Computational fluid dynamics (CFD) has been developed primarily to describe the flow of air as an ideal gas and of constant density liquids. The conservation equations of mass, momentum, and energy, when simplified to describe such flows, are solved with a variety of numerical techniques. The complexities arising from including turbulence, fluid property variation and reactions, and multi-phase flows in the simulations have not been addressed in a systematic fashion. However, enough work has been accomplished, and some of it made available as leased computational software that basic computational methodology can be identified. A critique of these models is shown in the following. These models may aptly be called computational transport phenomena (CTP), due to their applicability to multi-component and multi-phase flows. The models are meant to be illustrative only. A definitive critique is not possible due to commercial analytical codes and company codes being proprietary and to the current position of the government being to suppress federally funded research activities.

2. The scope of computational transport phenomena

Two basic approaches are used to formulate the conservation equations for modeling complex chemical processes. Firstly, a balance on an arbitrary control volume yields the transport equations for the property, Ψ:

$$\frac{\partial \Psi}{\partial t} + \nabla \cdot (\vec{v}\Psi) = \nabla \cdot \Omega + \sigma$$

where Ω is a tensor of order one greater than Ψ and σ. For momentum transport, Ψ the momentum vector, $\rho\vec{v}$, Ω the shear and normal stress tensor, $\hat{\tau} - \hat{I} \times P$, and the source term, σ, is a body force like gravity, $\rho\vec{g}$. The property Ψ may also represent mass, species concentrations, and energy, as will be illustrated subsequently.

The second approach is to use a population balance model:

$$\frac{\partial \Psi}{\partial t} + \nabla \cdot \vec{v}\Psi = -\frac{\partial}{\partial \vec{\zeta}} \cdot \vec{u}\Psi + B - D, \quad \text{where } u_i = \frac{\mathrm{d}\zeta_i}{\mathrm{d}t}$$

where the u_i''s are particle (or molecule or drop, etc.) characteristics defined by the internal coordinates, ζ_i. Such a model is integrated over time, space and the internal coordinates to define the system. B and D are birth and death functions of the particles, i.e. a generalized reaction rate.

These approaches are defined as deterministic systems by Himmelblau and Bischoff, *Process Analysis and Simulation*. These partial differential equations describe the process at a point and must be integrated over a volume to represent the entire system. The integration requires the use of initial/boundary conditions, and yields values of Ψ at each point in three-dimensional space for either steady or unsteady flow. Historically, these equations have been simplified by assuming geometrically simple, usually steady-state flow conditions. CFD allows us to represent the process without making these simplifying assumptions. CFD simulations are numerical solutions obtained for a discrete number of grid points. Before a discussion of grids is presented, variations of the basic model equations will be shown in order to demonstrate the generality and options available for modeling complex processes.

2.1. Laminar flows

To initiate our discussion, laminar flow of a multi-component, single-phase fluid will be described in a fixed coordinate system by the following. Cross-diffusion effects and non-Newtonian fluids are not considered at this point. These models are discussed extensively in Bird, Stewart, and Lightfoot, *Transport Phenomena* (2nd ed.).

The general balance equation:

$$\iiint \left[\frac{\partial \beta}{\partial t} + \nabla \cdot \beta \times \vec{W} + \nabla \cdot \vec{J} - \omega \right] \mathrm{d}\forall = 0, \quad \text{if } \beta \text{ is a scalar, or}$$

$$\iiint \left[\frac{\partial \vec{\beta}}{\partial t} + \nabla \cdot \vec{\beta} \times \vec{W} + \nabla \cdot \hat{J} - \vec{\omega} \right] \mathrm{d}\forall = 0, \quad \text{if } \beta \text{ is a vector}$$

The continuity equation:

$$\iiint \left[\frac{\partial \rho}{\partial t} + \nabla \cdot \rho \times \vec{U} \right] \mathrm{d}\forall = 0$$

The momentum equation:

$$\iiint \left[\frac{\partial \rho \times \vec{U}}{\partial t} + \nabla \cdot \rho \times \vec{U} \times \vec{U} + \nabla \cdot (P \times \hat{I} - \hat{\tau}) - \rho \times \vec{g} \right] d\forall = 0$$

The thermal energy equation:

$$\iiint \left[\frac{\partial \rho \times h \times \vec{U}}{\partial t} + \nabla \cdot (\rho \times h \times \vec{U}) - \frac{\mathrm{D}P}{\mathrm{D}t} + \nabla \cdot \vec{q} - \hat{\tau} : \nabla \vec{U} - \sum_k \vec{j}_k \cdot \vec{g} \right] \mathrm{d}\forall = 0$$

The species continuity equation:

$$\iiint \left[\frac{\partial \rho_i}{\partial t} + \nabla \cdot \rho_i \times \vec{U} + \nabla \cdot \vec{j}_i - \omega_i \right] \mathrm{d}\forall = 0$$

where

$$\hat{\tau} = +\mu(\nabla \vec{U} + (\nabla \vec{U})^{\mathrm{T}}) - \left(\tfrac{2}{3}\mu - b \right) (\nabla \cdot \vec{U}) \hat{\delta}$$

$$\vec{j}_{\mathrm{im}} = -\rho D_{\mathrm{im}} \nabla \cdot \alpha_i$$

$$\vec{q} = -\kappa \nabla T + \sum_k h_k \times \vec{j}_k$$

and β is the property/unit volume, W the number or mass average velocity, J the diffusion with respect to W and ω is the rate of generation of β. ρ is density, U the mass average velocity, and h is specific enthalpy. The g is gravity. The subscripts i and k signify a species value. The arrow overbar signifies a vector, and $\hat{\mathrm{i}}$s a second-order tensor. μ and b are the first and second coefficients of viscosity, respectively. κ is the thermal conductivity, and D_{im} is the multi-component diffusion coefficient. α_i is the mass fraction.

2.2. Turbulent flows

Numerous methods of turbulence modeling are continuously under investigation. The most fruitful is to average the laminar conservation equations over time. If the fluid density is constant, the time-average method of Reynolds (1895) is appropriate. For variable fluid density, the mass average method of Favre is useful. Physically, turbulence causes the fluid to act as though it has a very high viscosity (and conductivity and diffusivity) except near solid surfaces, where these transport mechanisms are reduced to laminar levels in very short distances. Conservation equations in this section are shown in terms of rectangular Cartesian coordinates. These models are discussed in Kuo, *Principles of Combustion*.

2.2.1. Reynolds averaging (time-averaging)

$$\bar{\phi} = \lim \frac{1}{\Delta t} \int_{t_\mathrm{o}}^{t_\mathrm{o}+\Delta t} \phi(t)\, \mathrm{d}t$$

$$\phi = \bar{\phi} + \phi'$$

Instantaneous value = average value + fluctuating value.

Rules for time-averaging:

$$\bar{\phi} = \langle \phi \rangle = \langle \bar{\phi} + \phi' \rangle \Rightarrow \bar{\phi}' = 0$$

$$\langle \phi + \psi \rangle = \bar{\phi} + \bar{\psi}$$

$$\langle \phi\psi \rangle = \bar{\phi}\bar{\psi} + \langle \phi'\psi' \rangle$$

$$\left\langle \frac{\partial \phi}{\partial X_i} \right\rangle = \frac{\partial \bar{\phi}}{\partial X_i}$$

$$\left\langle \int \phi \mathrm{d}X_i \right\rangle = \int \overline{\phi} \mathrm{d}X_i$$

2.2.2. Favre averaging (mass-averaging)

$$\tilde{\phi} = \frac{\langle \rho\phi \rangle_m}{\overline{\rho}}$$

$$\phi = \tilde{\phi} + \phi''$$

Instantaneous value = mass-average value + fluctuating value density is time-averaged.

Rules for mass-averaging:

$$\langle \rho\phi \rangle_m = \left\langle \rho \left(\tilde{\phi} + \phi'' \right) \right\rangle_m = \overline{\rho}\tilde{\phi} + \left\langle \rho\phi'' \right\rangle_m \Rightarrow \left\langle \rho\phi'' \right\rangle_m = 0$$

$$\tilde{\phi} - \overline{\phi} = -\overline{\phi}'' = \frac{\left\langle \rho'\phi'' \right\rangle_m}{\overline{\rho}} = \frac{\left\langle \rho'\phi' \right\rangle_m}{\rho'}$$

$$\left\langle \frac{\partial \rho\phi}{\partial X_i} \right\rangle_m = \frac{\partial \langle \rho\phi \rangle_m}{\partial X_i} = \frac{\partial \overline{\rho}\tilde{\phi}}{\partial X_i}$$

$$\left\langle \int \rho\phi \mathrm{d}X_i \right\rangle_m = \int \langle \rho\phi \rangle_m \mathrm{d}X_i = \int \overline{\rho}\tilde{\phi} \mathrm{d}X_i$$

Entire quantity in broken brackets is averaged. The subscript *m* denotes mass average, otherwise the term is time-averaged.

2.2.3. Incompressible turbulent transport equations

Dependent variables:

$$U_x = \overline{U}_x + U'_x; \quad U_y = \overline{U}_y + U'_y; \quad U_z = \overline{U}_z + U'_z; \quad P = \overline{P} + P'$$

Continuity:

$$\frac{\partial \overline{U}_x}{\partial x} + \frac{\partial \overline{U}_y}{\partial y} + \frac{\partial \overline{U}_z}{\partial z} = 0$$

x-Momentum:

$$\rho \left[\frac{\partial \overline{U}_x}{\partial t} + \overline{U}_x \frac{\partial \overline{U}_x}{\partial x} + \overline{U}_y \frac{\partial \overline{U}_x}{\partial y} + \overline{U}_z \frac{\partial \overline{U}_x}{\partial z} \right] = -\frac{\partial \overline{P}}{\partial x} + \nabla \cdot \left(\mu \nabla \overline{U}_x \right) - \rho \left[\frac{\partial \langle U'_x U'_x \rangle}{\partial x} + \frac{\partial \langle U'_x U'_y \rangle}{\partial y} + \frac{\partial \langle U'_x U'_z \rangle}{\partial z} \right] + \rho g_x$$

y-Momentum:

$$\rho \left[\frac{\partial \overline{U}_y}{\partial t} + \overline{U}_x \frac{\partial \overline{U}_y}{\partial x} + \overline{U}_y \frac{\partial \overline{U}_y}{\partial y} + \overline{U}_z \frac{\partial \overline{U}_y}{\partial z} \right] = -\frac{\partial \overline{P}}{\partial y} + \nabla \cdot (\mu \nabla \overline{U}_y) - \rho \left[\frac{\partial \langle U'_y U'_x \rangle}{\partial x} + \frac{\partial \langle U'_y U'_y \rangle}{\partial y} + \frac{\partial \langle U'_y U'_z \rangle}{\partial z} \right] + \rho g_y$$

z-Momentum:

$$\rho \left[\frac{\partial \overline{U}_z}{\partial t} + \overline{U}_x \frac{\partial \overline{U}_z}{\partial x} + \overline{U}_y \frac{\partial \overline{U}_z}{\partial y} + \overline{U}_z \frac{\partial \overline{U}_z}{\partial z} \right] = -\frac{\partial \overline{P}}{\partial z} + \nabla \cdot (\mu \nabla \overline{U}_z) - \rho \left[\frac{\partial \langle U'_z U'_x \rangle}{\partial x} + \frac{\partial \langle U'_z U'_y \rangle}{\partial y} + \frac{\partial \langle U'_z U'_z \rangle}{\partial z} \right] + \rho g_z$$

2.2.4. Compressible turbulent transport equations

Dependent variables:

$$U_x = \tilde{U}_x + U''_x; \quad U_y = \tilde{U}_y + U''_y; \quad U_z = \tilde{U}_z + U''_z; \quad P = \overline{P} + P'; \quad \rho = \overline{\rho} + \rho'$$

Continuity:

$$\frac{\partial \bar{\rho}}{\partial t} + \frac{\partial \bar{\rho}\tilde{U}_x}{\partial x} + \frac{\partial \bar{\rho}\tilde{U}_y}{\partial y} + \frac{\partial \bar{\rho}\tilde{U}_z}{\partial z} = 0$$

x-Momentum:

$$\left[\frac{\partial \bar{\rho}\tilde{U}_x}{\partial t} + \frac{\partial \bar{\rho}\tilde{U}_x\tilde{U}_x}{\partial x} + \frac{\partial \bar{\rho}\tilde{U}_x\tilde{U}_y}{\partial y} + \frac{\partial \bar{\rho}\tilde{U}_x\tilde{U}_z}{\partial z}\right] = -\frac{\partial \bar{P}}{\partial x} + \nabla\cdot(\mu\nabla\tilde{U}_x) - \left[\frac{\partial\langle\bar{\rho}U_x''U_x''\rangle_m}{\partial x} + \frac{\partial\langle\bar{\rho}U_x''U_y''\rangle_m}{\partial y} + \frac{\partial\langle\bar{\rho}U_x''U_z''\rangle_m}{\partial z}\right] + \bar{\rho}g_x$$

y-Momentum:

$$\left[\frac{\partial \bar{\rho}\tilde{U}_y}{\partial t} + \frac{\partial \bar{\rho}\tilde{U}_y\tilde{U}_x}{\partial x} + \frac{\partial \bar{\rho}\tilde{U}_y\tilde{U}_y}{\partial y} + \frac{\partial \bar{\rho}\tilde{U}_y\tilde{U}_z}{\partial z}\right] = -\frac{\partial \bar{P}}{\partial y} + \nabla\cdot(\mu\nabla\tilde{U}_y) - \left[\frac{\partial\langle\bar{\rho}U_y''U_x''\rangle_m}{\partial x} + \frac{\partial\langle\bar{\rho}U_y''U_y''\rangle_m}{\partial y} + \frac{\partial\langle\bar{\rho}U_y''U_z''\rangle_m}{\partial z}\right] + \rho g_y$$

z-Momentum:

$$\left[\frac{\partial \bar{\rho}U_z}{\partial t} + \frac{\partial \bar{\rho}\tilde{U}_z\tilde{U}_x}{\partial x} + \frac{\partial \bar{\rho}\tilde{U}_z\tilde{U}_y}{\partial y} + \frac{\partial \bar{\rho}\tilde{U}_z\tilde{U}_z}{\partial z}\right] = -\frac{\partial \bar{P}}{\partial z} + \nabla\cdot(\mu\nabla\tilde{U}_z) - \left[\frac{\partial\langle\bar{\rho}U_z''U_x''\rangle_m}{\partial x} + \frac{\partial\langle\bar{\rho}U_z''U_y''\rangle_m}{\partial y} + \frac{\partial\langle\bar{\rho}U_z''U_z''\rangle_m}{\partial z}\right] + \rho g_z$$

2.2.5. Turbulence parameters

Turbulent intensity:

$$I_i = \frac{(\langle U_i'U_i'\rangle)^{0.5}}{U}, \quad \text{for} \quad i = x, y, z, \quad I_{\mathrm{TOT}} = \frac{(\langle U_x'U_x'\rangle + \langle U_y'U_y'\rangle + \langle U_z'U_z''\rangle)^{0.5}}{U\sqrt{3}}$$

Turbulent kinetic energy:

$$k = 0.5\sum_i \langle U_i'U_i'\rangle \quad \text{or} \quad 0.5\sum \frac{\langle \rho U_i''U_i''\rangle_m}{\bar{\rho}}$$

- High Reynolds k–ε model for eddy viscosity:

$$\mu_t = \frac{C_\mu \bar{\rho}k^2}{\varepsilon}$$

- Transport equation for k:

$$\frac{\partial \bar{\rho}k}{\partial t} + \sum_i \frac{\partial \bar{\rho}\tilde{U}_i k}{\partial X_i} = \sum_j \frac{\partial}{\partial X_j}\left[(\mu + \mu_t)\frac{\partial k}{\partial X_j}\right] + \sum_i\sum_j \tau_t \frac{\partial \tilde{U}_i}{\partial X_j} - \bar{\rho}\varepsilon$$

- Transport equation for ε:

$$\frac{\partial \bar{\rho}\varepsilon}{\partial t} + \sum_i \frac{\partial \bar{\rho}\tilde{U}_i \varepsilon}{\partial X_i} = \sum_j \frac{\partial}{\partial X_j}\left[(\mu + 0.77\mu_t)\frac{\partial \varepsilon}{\partial X_j}\right] + C_{\varepsilon_1}\frac{\varepsilon}{k}\sum_i\sum_j \tau_t \frac{\partial \tilde{U}_i}{\partial X_j} - \frac{C_{\varepsilon_2}\bar{\rho}\varepsilon^2}{k}$$

where $C_{\varepsilon_1} = 1.44$, $C_{\varepsilon_2} = 1.92$, and $C_\mu = 0.09$, and $\tau_i = -\langle \rho U_i''U_j''\rangle \approx a\bar{\rho}k$

- For the k–ε turbulence model, the Reynolds stress becomes:

$$\tau_t = -\left\langle \bar{\rho}U_i''U_j''\right\rangle_m = \mu_t\left(\frac{\partial \tilde{U}_i}{\partial X_j} + \frac{\partial \tilde{U}_j}{\partial X_i}\right) - \left(\frac{2}{3}\right)\delta_{ij}\left(\bar{\rho}k + \mu_t\frac{\partial \tilde{U}_k}{\partial X_k}\right)$$

δ_{ij} is Kronecker delta; it equals 1 if $i = j$, otherwise it equals 0. Since this equation is in Cartesian tensor nomenclature, the repeated index k indicates a summation over the X_k coordinates.

2.2.6. The turbulent energy equation

- Mass average variables:

$$h = \tilde{h} + h''; \quad e = \tilde{e} + e''; \quad T = \tilde{T} + T''; \quad \tilde{h} = \frac{\langle \rho h\rangle_m}{\bar{\rho}}; \quad \tilde{e} = \frac{\langle \rho e\rangle_m}{\bar{\rho}}; \quad \tilde{T} = \frac{\langle \rho T\rangle_m}{\bar{\rho}}$$

- Thermal energy equation:

$$\frac{\partial \overline{\rho}\tilde{h}}{\partial t} + \sum_i \frac{\partial \overline{\rho}\tilde{U}_i\tilde{h}}{\partial X_i} = \frac{\partial \overline{P}}{\partial t} + \sum \tilde{U}_i \frac{\partial \overline{P}}{\partial X_i} + \sum \left\langle U_i'' \frac{\partial P'}{\partial X_i} \right\rangle_m - \sum_i \frac{\partial \overline{q}_i}{\partial X_i} - \sum \frac{\partial}{\partial X_i} \langle \overline{\rho} U_i'' i'' \rangle_m - \sum_i \sum_j \left[\overline{\tau}_{ij} \frac{\partial \tilde{U}_i}{\partial X_j} + \left\langle \tau_{ij} \frac{\partial U_i''}{\partial X_j} \right\rangle_m \right]$$

- Heat flux:

$$\overline{q}_j = -\kappa \frac{\partial \tilde{T}}{\partial X_j} - \sum_{j=1}^{n} \frac{\mu}{Sc} \left(\tilde{h}_i \frac{\partial \tilde{\alpha}_i}{\partial X_j} \right) = -C_p \frac{\mu}{Pr} \frac{\partial \tilde{T}}{\partial X_j} - \sum_{j=1}^{n} \frac{\mu}{Sc} \left(\tilde{h}_i \frac{\partial \tilde{\alpha}_i}{\partial X_j} \right)$$

The time-averaged energy equation contains terms, which have not yet been modeled.

- Averaging with filter functions (G)

Linear and time averaging for constant density flow (has not yet been applied to multi-dimensional flows). Ref. Dakhoul, Improved averaging method for turbulent flow simulation (dissertation).

$$\langle \Psi(\vec{x}, t) \rangle = \int G(\vec{x} - \vec{x}', t - t') \times \Psi(\vec{x}', t') \times \mathrm{d}\vec{x}' \mathrm{d}t'$$

Linear averaging for constant density flow (Leonard's filter):

$$\langle \vec{U}(\vec{x}, t) \rangle = \int G(\vec{r}, \vec{x}) \vec{U}(\vec{x} - \vec{r}) \mathrm{d}\vec{r}, \quad \text{where} \quad \int G(\vec{r}, \vec{x}) d\vec{r} = 1$$

Filter functions are discussed in Pope, *Turbulent Flows*. Filter functions are used to introduce an eddy size into turbulence models, thereby producing large eddy simulation (LES) methodology. LES models are not now computationally practical.

3. Multi-phase flows

For a fluid continuum with a sparse distribution of particulates (solids, bubbles or droplets), Euler–Lagrange methods may be used. The fluid flow is calculated then the particles are tracked through the flowfield. However, if the distribution of particulates is dense, both phases are more strongly coupled and the flow is more efficiently simulated with strictly Eulerian methods. These methods are described as follows.

3.1. Volume averaging

Consider the volume averaging developed by Whitaker, "The transport equations for multi-phase systems," *CES*, vol. 28. The size of the particles relative to the size of the system is described with several scales for two phases:

scale: $d \ll l \ll L$;
phases: α and β;
volumes: $\forall = \forall_\alpha + \forall_\beta$;
spatial average: $\langle \Psi \rangle = \frac{1}{\forall} \int_\forall \Psi \mathrm{d}\forall$;
phase average: $\langle \Psi_\alpha \rangle = \frac{1}{\forall} \int_{\forall_\alpha} \Psi \mathrm{d}\forall$;
intrinsic phase average: $\langle \Psi_\alpha \rangle^\alpha = \frac{1}{\forall_\alpha} \int_{\forall_\alpha} \Psi \mathrm{d}\forall$;
volume fraction: $\varepsilon_\alpha = \frac{\langle \Psi_\alpha \rangle}{\langle \Psi_\alpha \rangle^\alpha}$.

Averaged transport equation:

$$\varepsilon_\alpha \left(\frac{\partial \langle \Psi_\alpha \rangle^\alpha}{\partial t} \right) + \langle \Psi_\alpha \rangle^\alpha \left(\frac{\partial \varepsilon_\alpha}{\partial t} \right) + \nabla \cdot (\varepsilon_\alpha \langle \vec{v}_\alpha \rangle \langle \Psi_\alpha \rangle^\alpha) + \nabla \cdot \langle \tilde{\vec{v}}_\alpha \tilde{\Psi}_\alpha \rangle + \frac{1}{\forall} \int_{A_{\alpha\beta}} \Psi_\alpha (\vec{v}_\alpha - \vec{w}_\alpha) \cdot \mathrm{d}\vec{A}_\alpha = \nabla \cdot \langle \Omega_\alpha \rangle + \frac{1}{\forall} \int_{A_{\alpha\beta}} \Omega_\alpha \cdot \mathrm{d}\vec{A}_\alpha + \varepsilon_\alpha \langle \Psi_\alpha \rangle^\alpha$$

where w is the velocity of the interface A_α, between the phases. $A_{\alpha\beta}$ is the interfacial area of both phases in the averaged volume.

The volume averaging procedure is quite similar to the spatial filtering methods used to represent turbulent flow. These methods are discussed at length in Slattery, *Momentum, Energy, and Mass Transfer in Continua*.

3.2. Multi-phases as coexisting continua

Just as multi-component flows are treated as being continua in each component, multi-phase flows may be treated as being coexisting continua in each phase. This allows us to write the Eulerian transport equations for each phase, including interaction terms between the phases, and solve the entire set to represent the process. This was accomplished by Anderson and Jackson, *IEC Fundamentals*, vol. 6 to simulated fluidized beds. A recent evaluation of this methodology is reported by van Wachem et al. in *AIChE Journal*, vol. 47.

Continuity:

$$\frac{\partial \varepsilon_g}{\partial t} + \nabla \cdot (\varepsilon_g \vec{v}_g) = 0$$

$$\frac{\partial \varepsilon_s}{\partial t} + \nabla \cdot (\varepsilon_s \vec{v}_s) = 0$$

Momentum (from Jackson):

$$\rho_g \left[\frac{\partial \vec{v}_g}{\partial t} + \vec{v}_g \cdot \nabla \vec{v}_g \right] = \nabla \cdot \hat{\tau}_g - \nabla P - \frac{\beta}{\varepsilon_g}(\vec{v}_g - \vec{v}_s) + \rho_g \vec{g}$$

$$\rho_s \varepsilon_s \left[\frac{\partial \vec{v}_s}{\partial t} + \vec{v}_s \cdot \nabla \vec{v}_s \right] - \rho_g \varepsilon_s \left[\frac{\partial \vec{v}_g}{\partial t} + \vec{v}_g \cdot \nabla \vec{v}_g \right] = \nabla \cdot \hat{\tau}_s - \nabla P_s + \frac{\beta}{\varepsilon_g}(\vec{v}_g - \vec{v}_s) + \varepsilon_s(\rho_s - \rho_g)\vec{g}$$

The details of the modeled terms have not yet been universally accepted, but the general methodology has been developed and is subject to investigation by current simulation studies.

3.3. The relationship between PDFs and transport models

The concepts used in statistical mechanics can be used to represent flows of molecules or multi-phase flows consisting of fluid/particulate mixtures. The derived conservation equations may be solved directly or modeled transport equations may be solved for the probability density functions.

3.3.1. Transport equations from a PDF

The Boltzmann equation for the velocity distribution function (for monatomic, non-reacting mixtures of low-density gases). The concept of phase space, i.e. position and velocity.

$$\frac{\partial}{\partial t} f_\alpha = -\left(\frac{\partial}{\partial \vec{r}} \cdot \dot{\vec{r}}_\alpha \times f_\alpha \right) - \left(\frac{\partial}{\partial \dot{\vec{r}}_\alpha} \cdot \vec{g}_\alpha \times f_\alpha \right) + J_\alpha$$

Weighing the Boltzmann equation by a molecular property and integrating over all of the molecular velocities:

$$\frac{\partial}{\partial t} \int \Psi_\alpha \times f_\alpha \times \mathrm{d}\dot{\vec{r}}_\alpha = -\left(\frac{\partial}{\partial \vec{r}} \cdot \int \dot{\vec{r}}_\alpha \times \Psi_\alpha \times f_\alpha \times \mathrm{d}\dot{\vec{r}}_\alpha \right) + \int \left(\vec{g}_\alpha \cdot \frac{\partial \Psi_\alpha}{\partial \dot{\vec{r}}_\alpha} \right) f_\alpha \times \mathrm{d}\dot{\vec{r}}_\alpha + \int \Psi_\alpha \times J_\alpha \times \mathrm{d}\dot{\vec{r}}_\alpha$$

for Ψ_α = mass (m_α), momentum ($m_\alpha \dot{\vec{r}}_\alpha$), and energy ($0.5 m_\alpha (\dot{\vec{r}}_\alpha \cdot \dot{\vec{r}}_\alpha)$), respectively, the laminar, non-reacting transport equations result.

When the fluid is in motion, the distribution function must be corrected. When this is done, expressions for the laminar transport coefficients can be obtained.

Similar expressions can be obtained for polyatomic gases, monatomic liquids, and polymeric liquids. However, no new information is generated which is not already available in the phenomenological statement of the transport equations. These equations are discussed in Bird, Stewart, and Lightfoot, *Transport Phenomena* (2nd ed.).

3.3.2. Application of PDF methods to particulate flows

Even if the particulates are not molecular in scale, the same statistical methods may be applied to their analysis. Hulbert and Katz, "Some problems in particle technology," *CES*, vol. 19, 1962 addressed this application by introducing x_i's as external

coordinates and ζ_j's as internal coordinates of the property Ψ. The internal coordinates are used to simulate the physical processes, which the particles are undergoing.

$$\int_R \left\{ \frac{\partial \Psi}{\partial t} + \sum_{k=1}^{3} \frac{\partial}{\partial x_k}(v_k \times \Psi) + \sum_{j=1}^{m} \frac{\partial}{\partial \zeta_j}(u_j \times \Psi) + D - B \right\} \mathrm{d}\vec{R} = 0$$

To simplify the simulation, the integration over the internal coordinates was accomplished by using the method of moments. Applications are discussed in Randolph and Larson, *Theory of Particulate Processes*. Such methods are still under investigation; Verkoeijen et al., "Population balances for particulate processes: A volume approach," *CES*, vol. 57, 2002. As with most chemical process analyses, such research has been primarily directed at investigating the physical processes the particulates are encountering while over simplifying their motion, i.e. assuming the velocity field or restricting its geometric variation.

3.3.3. Application of PDF methodology to turbulent flows

With a goal of getting more detail into the analysis of turbulent flows, investigators have stopped short of averaging the laminar flow conservation equations to initiate their analyses. Instead, they solve a transport equation for the PDF or approximate the PDF from experimental data. To date, such modeling approaches have not produced practical process simulation models, although they have contributed to a more basic understanding of turbulent flows.

The PDF transport equation for incompressible flow:

$$\frac{\partial f}{\partial t} + V_i \frac{\partial f}{\partial x_i} = \frac{1}{\rho} \frac{\partial \langle p \rangle}{\partial x_i} \frac{\partial f}{\partial V_i} - \frac{\partial}{\partial V_i} \left[f \left[\left\langle \nu \nabla^2 U_i - \frac{1}{\rho} \frac{\partial p'}{\partial x_i} \,|\, \vec{V} \right\rangle \right] \right]$$

The evolution of the moments of "f" yield the velocity $\langle \vec{U} \rangle$ and $\langle u_j u_k \rangle$. These methods are well presented by Pope, *Turbulent Flows*. Extension to the description of reacting flows has been accomplished by Fox, *Computational Models for Turbulent Reacting Flows*. Realistic variation of density and complex chemical reactions has not yet been addressed with these methods. In the opinion of these investigators, the inclusion of density variations in the description of turbulent reacting flows is more important than the description of local unmixedness, which is obtained from the use of PDF methodology. Admittedly, adequate experimental justification of the relative importance of these effects is not available. However, chemical kinetics are determined by experiment, not theory. If unmixedness is important, in all likelihood, it also affected the reported experimental reaction rates. In any event, the computational efficiency of using PDF methodology precludes it from being a practical process simulation tool at this time.

4. Coordinates and grids

To solve the conservation equations numerically for a complex flow, a grid system is needed. Simple orthogonal grids are described in Bird, Stewart, and Lightfoot, *Transport Phenomena* (2nd ed.). In practice, general curvilinear grids are used; such grids are discussed in Fletcher, *Computational Techniques for Fluid Dynamics, vol. II*. The extensive research on grids performed at Mississippi State University is contained in the tome *Handbook of Grid Generation* edited by Thompson, Soni, and Weatherill. Almost never will the very general grids developed to describe flow about aircraft be needed for process analyses. However, if environmental phenomena related to toxic releases or explosive accidents are simulated, the general grid methods should be considered. Moving grids are of great benefit for such simulations. What is needed is an elementary grid generator for curvilinear coordinates, which can be used to understand CFD analyses of transport phenomena.

Ultimately, a grid generator for physical curvilinear moving coordinates should be developed as a public-domain tool. A start in developing such a grid generator is reported by Lee and Soni, "Governing Equations of Fluid Mechanics in Physical Curvilinear Coordinate System," *Electronic Journal of Differential Equations* (1997). Elaborate grid generators are not needed except to match the geometry of the process system. However, if an elementary grid code is available, its use is transparent to the practitioner. An additional benefit for using such coordinates is that tensor quantities are elegantly defined. Much of the transport literature is confusing on the definition and use of tensor analysis.

For constant density flow, the conservation equations physical coordinates are:

$$\frac{\partial}{\partial \xi^i} \left(\frac{J}{\sqrt{g_{ii}}} u^{(i)} \right) = 0$$

$$R_{\text{eff}}\frac{\partial u^{(i)}}{\partial t}+R_{\text{eff}}v^{(j)}\left(\frac{\partial u^{(i)}}{\partial \xi^{(j)}}+u^{(k)}\Gamma^{i}_{kj}\right)=-R_{\text{eff}}\left[g^{(ij)}\frac{\partial P}{\partial \xi^{(j)}}-\frac{\partial \nu_E}{\partial \xi^{(j)}}\left[g^{(jk)}\frac{\partial u^{(i)}}{\partial \xi^{k}}+g^{(jk)}\Gamma^{(i)}_{(lk)}u^{(l)}+g^{(ik)}\frac{\partial u^{(i)}}{\partial \xi^{k}}+g^{(ik)}\Gamma^{j}_{lk}u^{(l)}\right]\right]$$
$$+g^{(jk)}\left[\frac{\partial^2 u^{(i)}}{\partial \xi^{(k)}\partial \xi^{(j)}}+\frac{\partial(u^{(l)}\Gamma^{i}_{lj})}{\partial \xi^{(k)}}+\Gamma^{i}_{lk}u^{(l)}_{,(j)}-\Gamma^{l}_{jk}u^{i}_{,l}\right]$$

The major advantage in simulating transport phenomena in multiple dimensions is that the quantitative effect of approximating these flows with simplified geometry can be evaluated.

5. Non-Newtonian flows

Many process flows are non-Newtonian, such as polymeric flow and flows of suspensions. However, simulation of the shear rate–shear stress can be only described with simple models, such as power law models. Laminar flows to interpret rheological experiments have been extensively modeled (for example, see BSL, *Transport phenomena*, 2nd ed.). The co-rotating and codeforming derivatives used in such models cannot be conveniently utilized to model process flows. In the first place, only differential and partial differential equations have established solution methodology. In the second place, only basic non-Newtonian flows have been investigated in the turbulent flow regime.

6. Examples

These investigators endorse the use of computational transport phenomena models for the practical analysis complex chemical processes. For multi-component reacting flows, modest sized kinetics mechanisms can be analyzed with current methodology. Since kinetics models are experimentally determined, large kinetics models cannot be sufficiently validated to be justified, nor are they computationally efficient to analyze. Variable fluid properties can be easily included in the analysis. For multi-phase flows, additional interaction terms can be easily included in the computational analysis. The problem is one of validation. Using more elaborate models than can be validated is misleading and often renders the simulation impractical. Two-equation turbulence models have been shown to be very useful in simulations. More elaborate DNS, LES, and PDF turbulent simulations are not computationally practical. Two examples are presented in the following to justify this position.

6.1. Stirred-tank reactors

Agitated vessels are widely used in the chemical, pharmaceutical, and petroleum refinery industries for mixing and chemical processing. An impeller is used to generate a turbulent flowfield which minimizes temperature and concentration gradients, suspends solid particles, maintains emulsions, disperses a gas into a liquid, and combines chemical reactants. Two complementary simulation and validation investigations were conducted by the Chemical Engineering Department at Louisiana State University to model these stirred-tank systems.

To model the flow in a baffled, tank stirred by a Rushton turbine impeller in which no reactions occurred, a CFD analysis was made and flowfield validation experiments were conducted. The geometry of this tank is shown in Fig. 1. The fluid studied

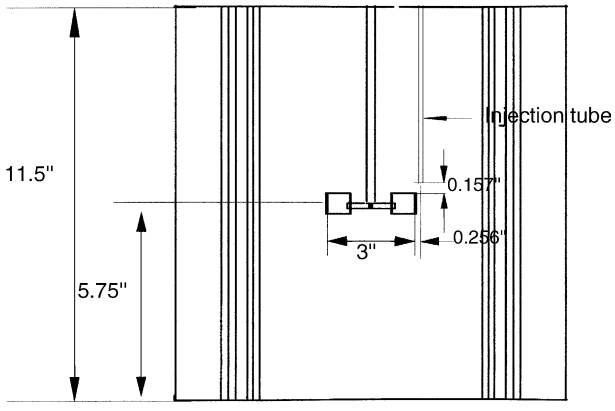

Fig. 1. Standard tank configuration with a Rushton turbine.

was dimethyl silocone. The turbulent flow was modeled with a CFD code based on the methods of Patanker and Spalding, *International Journal of Heat and Mass Transfer*, vol. 15, 1972. A non-uniform, three-dimensional, cylindrical grid was used to discretize a quadrant of the tank. Periodic boundary conditions were used to match the flows at the sides of the quadrants. No-slip conditions were applied at the tank and baffle surfaces. The fluid surface was assumed to be flat. Flow into and out of the turbine blade was represented as specified velocity profiles into the turbine hub region and out of the tip region. The turbulence properties were initially represented with a k–ε model. Notice, that the flow in the vicinity of the turbine blade and the fluid surface were simplified in order to keep the simulation practical.

The mean velocity field through out the tank was measured with a hot wire anemometer. The measurements indicated that the turbulent flowfield was non-isotropic. Since the k–ε model assumes isotropy, modifications to the model were made. The eddy viscosity was assumed to be a tensor function with the μ_{rz} component coming directly from the k–ε model. The other components were represented by:

$$\mu_{ij} = \frac{\mu_{rz}}{\sigma_{ij}},$$

where

$$\sigma_{r\theta} = \sigma_{\theta z} = \sigma_{rr} = \sigma_{\theta\theta} = \sigma_{zz} = 1, \quad \text{in the bulk region}$$

$$\sigma_{r\theta} = \sigma_{rr} = \sigma_{\theta\theta} = \sigma_{zz} = 0.7, \quad \text{in the impeller stream}$$

$$\sigma_{\theta z} = 1 + S^{1/3}, \quad \text{in the impeller stream}$$

where S is the swirl number.

The CFD simulation, with the improvement obtained by this non-isotropic model, agreed very well with the experimental test data.

The second investigation involved reacting flow in the same tank. Hydrochloric acid and sodium hydroxide were reacted. The hydroxide was injected near the turbine tip. Tomography was used to track the local concentrations and reacting flow front.

This flow was simulated with the leased Fluent CFD code. The grid and boundary conditions were the same as for the non-reacting case. The non-isentropic turbulence model could not be used because only the source code was available. However, the "renormalization group" (RNG) turbulence model was used. The RNG model is similar to the basic, isotropic k–ε model, except for three features: (1) the effective eddy viscosity is calculated from an ordinary differential equation; (2) there is an extra term in the dissipation rate equation; (3) there is a correction term to modify the eddy viscosity for swirling flow.ODE for eddy viscosity (to account for low *Re* effects):

$$\mathrm{d}\left(\frac{\rho^2 k}{\sqrt{\varepsilon\mu}}\right) = 1.72\frac{\widehat{\nu}}{\sqrt{\widehat{\nu}^3 + 99}}\mathrm{d}\widehat{\nu}, \quad \text{where } \widehat{\nu} = \frac{\mu_{\text{eff}}}{\mu}$$

Additional term in the dissipation equation source:

$$R_\varepsilon = \frac{C_\mu \rho \eta^3 (1 - \eta/4.38)}{1 + 0.012\eta^3}\frac{\varepsilon^2}{k}, \quad \text{where } \eta = \frac{Sk}{\varepsilon}$$

The swirl correction to the eddy viscosity is:

$$\mu_t = \mu_{\text{to}} f\left(\alpha_s, \Omega, \frac{k}{\varepsilon}\right) \quad \text{where } \alpha_s \text{ is a constant and } \Omega \text{ is a swirl number.}$$

The neutralization reaction was modified to reflect an empirical correction for concentration oscillation correlations.

The instantaneous point measurements made with tomography are shown in Fig. 2 for a point near the turbine tip. The time-averages of these measurements are compared to the time-average simulation in Fig. 3. Radial concentration predictions and measurements are shown in Fig. 4 for two elevations between the turbine blade and fluid surface. The radial velocity profile from the turbine blade tip to the wall is shown in Fig. 5. The transport model agreed with the measured data very well and was, therefore, considered to be validated.

6.2. Spray flames

The main combustion chamber on liquid rocket propelled launch vehicles, like that of the space shuttle main engine, consists of hundreds of individual injector elements which feed the fuel and oxidizer into the high-pressure chamber. To accurately predict the thrust generated and the thermal environment of the engine walls, the degree of local mixing and the extent of the combustion reactions must be established. These conditions cannot be measured experimentally. To be predicted by CTP

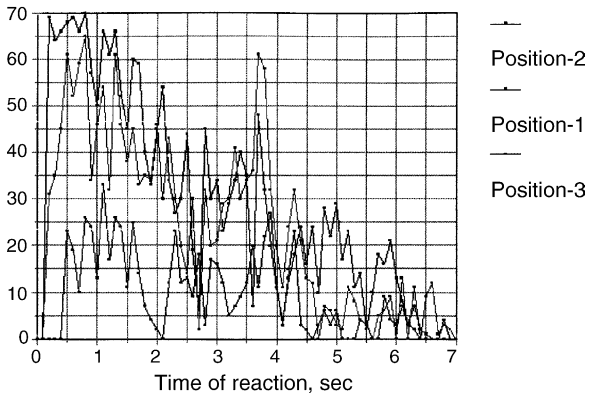

Fig. 2. Grid points concentration profiles.

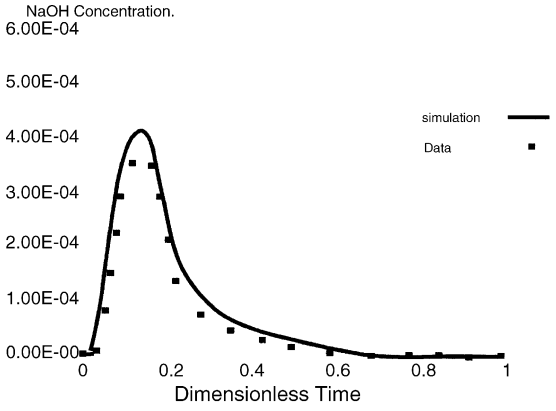

Fig. 3. Local point comparison of simulated NaOH concentration with time-averaged NaOH data at point 2 near the tip of impeller.

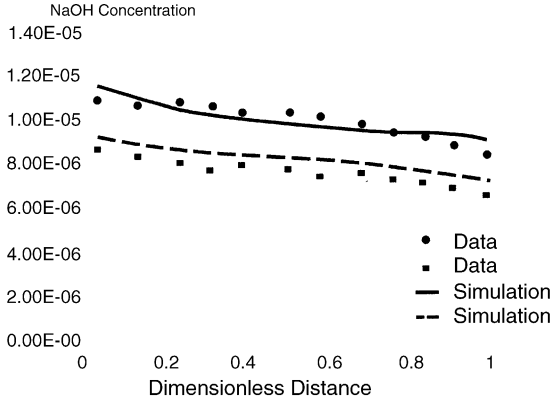

Fig. 4. Comparison of NaOH concentration as a function of dimensionless distance.

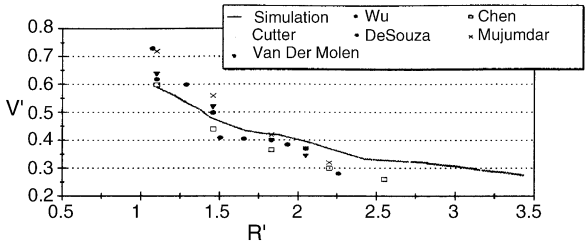

Fig. 5. A radial velocity profile in the impeller stream.

methods, the liquid flowrate and thermodynamic state exiting the injector element and the geometry and thermal structure of the wall are available as boundary conditions. Although spray flames have been investigated by experiment and analysis for more than 30 years, practical simulations of launch vehicle engines are not possible. These investigators proposed and sought validation for an engineering model, which provided the desired design tools.

The major problem in simulating dense spray flames is that the particle size and distribution created by the individual injector elements cannot be measured. This means that postulated spray formation models cannot be validated with respect to the initial mixing of the spray droplets. These investigators devised a new model of these processes based on reasonable, albeit approximate, physics of the spray. Many large rocket engine combustors operate at supercritical conditions; hence, even if droplets are present they would be unstable. Had the entering propellants been assumed to be gases, the local propellant enthalpy and mixing conditions would be erroneously simulated. Yet, such simulations have been used by the industry since the early 60s. The new spray model utilized a mature CFD code for turbulent, reacting flow and approximated the spray to be a homogeneous, real fluid whose thermodynamic properties accounted for the multi-phase flow effects. Thus, the local amount of liquid propellant was described in terms of the fluid quality. Initially, there was assumed to be no velocity or thermal lag between the phases. The plan was that: (1) thermal lags could be represented by "kinetics" models which delayed the transition of liquid droplets to gaseous globules and (2) that spray mixing rates could be adjusted by modifying the empirical turbulent transport coefficients to fit what ever data was to be used for the validation process. This spray model was implemented and tested by comparison to available test data. In short, the validation showed that the model was very reasonable with no modifications needed to account for thermal lags or mixing behavior. Even though the simulations were computationally intensive, the chamber mixing and local heat release in terms of injector design parameters were predictable for the first time. Subsequent improvements to the computational efficiency are being addressed. More importantly, testing parameters can now be identified which when measured can lead to improved simulation methodology.

Details of this new spray combustion model for high-pressure flames is described as follows. The FDNS–RFV CFD code was used to solve a set of non-linear, coupled conservation equations. Finite differences were employed to discretize the equations on a non-staggered grid. High-order up-wind, total variation diminishing (TVD) or second-order central differencing with second- or fourth-order dissipation was used to represent convective terms and stabilize shock structure, if any. Second-order central differencing was used to represent viscous and source terms. Vectorized point implicit, conjugate gradient, and generalized minimal residual matrix solvers were optionally employed to insure a stable, accurate, and fast convergence rate. Multi-block, multi-zone options were included to efficiently represent complex geometries. A pressure based predictor/multi-corrector was employed so that both compressible and incompressible flows could be simulated. A time-centered Crank–Nicholson or Euler implicit time-marching scheme was used for time-accurate discretization. For steady-state simulations, implicit Euler or explicit marching may be used. Options to account for either finite-rate or equilibrium chemistry are included. Real fluid properties are obtained from thermal and caloric equations of state. Turbulence is represented with either an incompressible (i.e. constant density) or compressible, two-equation k–ε model. Wall boundary conditions may be satisfied with direct integration to the wall or with wall functions.

The conservation equations solved in the general curvilinear coordinate system employed are as follows:

$$\frac{1}{J}\frac{\partial}{\partial t}(pq) + \frac{\partial}{\partial \xi_i}(\rho U_i q) = \frac{\partial}{\partial \xi_i}\left(\mu_e G_{ij}\frac{\partial q}{\partial \xi_j}\right) + S_q$$

where $q = l, u, v, w, h, k, \varepsilon$ and α_a.

$$U_i = \frac{u_j}{J}\frac{\partial \xi_i}{\partial x_j}, \quad \text{contra variant velocity}$$

$$G_{ij} = \frac{1}{J}\frac{\partial \xi_i}{\partial x_k}\frac{\partial \xi_j}{\partial x_k}, \quad \text{diffusion metric}$$

$$J = \frac{\partial(\xi, \eta, \zeta)}{\partial(x, y, z)}, \quad \text{the Jacobian}$$

$J = [x_\xi(y_\eta z_\zeta - y_\zeta z_\eta) - x_\eta(y_\xi z_\zeta - y_\zeta z_\xi) + x_\zeta(y_\xi z_\eta - y_\eta z_\xi)]^{-1}$.

The effective viscosity:

$$\mu_e = \frac{\mu + \mu_t}{\sigma_q} \quad \text{and} \quad \mu_t = \rho C_\mu \frac{k^2}{\varepsilon}$$

The source terms:

$$S_q = \frac{1}{J}\begin{vmatrix} 0 \\ -\dfrac{\partial p}{\partial x_i} + \dfrac{\partial \mu_e}{\partial x_j}\dfrac{\partial u_j}{\partial x_i} - \dfrac{2\lambda_c}{3}\dfrac{\partial \mu_e}{\partial x_i}\dfrac{\partial u_j}{\partial x_j} + \dfrac{\lambda_c}{3}\dfrac{\partial}{\partial x_j}\left(\mu_e \dfrac{\partial u_j}{\partial x_j}\right) + (1-\delta_{jk})\dfrac{\partial}{\partial \xi_j}\left(JG_{jk}\mu_e \dfrac{\partial u_i}{\partial \xi_k}\right) + F_i \\ \dfrac{\mathrm{D}p}{\mathrm{D}t} + \Phi + Q_t \\ \rho(P_r - \varepsilon) \\ \rho\dfrac{k}{\varepsilon}\left[\left(\dfrac{C_1 + C_3 P_r}{\varepsilon}\right)P_r - C_2\varepsilon\right] \\ \omega_a \end{vmatrix}$$

$\alpha = 1, \ldots, N$ are the number of species, $i = 1$–3 for the three momentum equations, δ_{jk} the Kronecker delta, $\lambda_c = 1.0$ for compressible and incompressible flow, respectively, σ_q the dimensionless transport coefficient, P_r the production rate of turbulent kinetic energy, F_i the body forces like buoyancy, Coriolis, and centrifugal forces, Φ the viscous dissipation and the Q_t the additional energy sources.The additional energy sources can be radiation, absorption of electrical energy, etc. Depending on the type source Q_t can be modeled in many different ways:

$$P_r = \frac{\mu_t}{\rho}\left[2(u_x^2 + v_y^2 + w_z^2) + (v_x + u_y)^2 + (w_y + v_z)^2 + (u_z + w_x)^2 - \frac{2\lambda_c}{3}(u_x + v_y + w_z)^2\right]$$

where the subscripts x–z indicate partial differentiation.

The pressure correction equation:

$$\frac{\beta_p p'}{\Delta t} + \nabla\cdot(u_i\beta_p p') - \nabla\cdot(\rho \times D_p \nabla p') = -\nabla\cdot(\rho \times u_i) - \frac{\rho * - \rho^n}{\Delta t}$$

$$p^{n+1} = p^n + p'$$

D_p is proportional to the magnitude of the matrix coefficients of the momentum equations. β_p is a parameter relating p and ρ; * denotes evaluation at an intermediate time; n denotes a value at a previous time.

Wall functions are used as boundary conditions.

A wall function model is used as a wall boundary condition so that coarser grid sizes can be tolerated close to the wall. The non-dimensional zed velocity u^+ is evaluated from the velocity profile:

$$u^+ = \ln\left[\frac{(y^+ + 11)^{4.02}}{(\{y^+\}^2 - 7.37y^+ + 83.3)^{0.79}}\right] + 5.63\tan^{-1}(0.12y^+ - 0.441) - 3.81$$

where $u^+ = u/u_\tau$, $y^+ = \rho u_\tau\, y/\mu$, and $u_\tau = (\tau_w/\rho)^{0.5}$. This velocity profile provides a smooth transition between the logarithmetic law of the wall and the linear viscous sublayer variation. For heat transfer, a wall function for heat flux is:

$$q_w = \frac{\rho u_\tau}{Pr_t u^+}\left[h_w - h_p - \sqrt[a]{Pr_t}\frac{(V_p - V_w)^2}{2}\right]$$

where V is total velocity, Pr_t is the turbulent Prandtl number, and the subscripts p and w denote values near the wall and at the wall, respectively. For laminar flows a is one-half and for turbulent flows a is one-third. For adiabatic walls, q_w is 0.

As previously mentioned, sufficiently detailed experiments to validate the new homogeneous spray combustion model are non-existent. The most appropriate validation data are from the participants of the International Workshops on Rocket Combustion Modeling (IWRCM). Test data were presented at the 2nd IWRCM for cold flow of nitrogen and hot flow of LOX and hydrogen at both subcritical and supercritical LOX pressures: all in a single axisymmetric coaxial injector element system. The FDNS–RFV code with the homogeneous spray combustion model was used to simulate these cases. At these high-pressures, chemical equilibrium of the combustion reactions should be obtained. Chemical equilibrium was assumed in the modeling process; however, a finite-rate simulation with a conventional eight-reaction mechanism for the H_2/O_2 system was also performed to verify this assumption.

The geometry and results of the subcritical combustion case are shown in Figs. 6–15. The simulation is shown to agree reasonably well with measured temperatures as shown in Figs. 7–12. But, since no error bounds were presented for the test data, detailed comparisons are difficult make. The radial temperature profile closest to the faceplate shows a temperature spike. Both

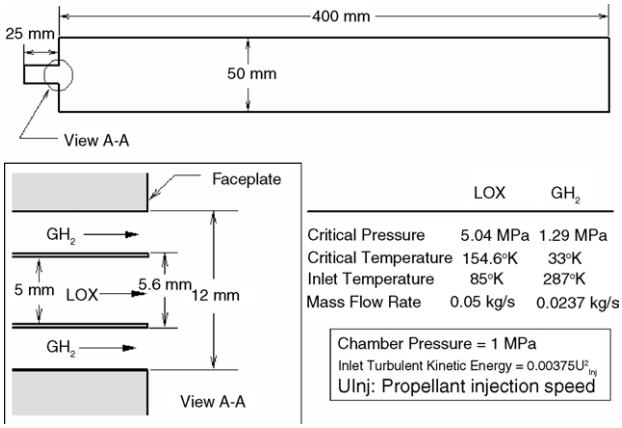

Fig. 6. Configuration and inlet flow conditions of the RCM-2 test case.

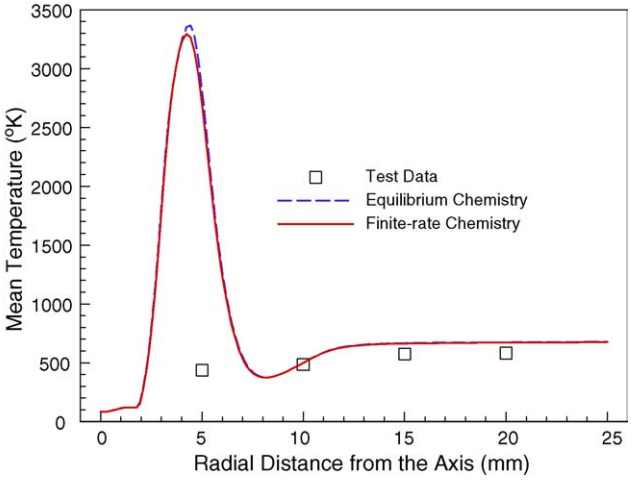

Fig. 7. Comparisons of temperature profile at $X/D = 2$, RCM-2 test case.

reaction schemes assumed all of the oxygen to be reacting with the hydrogen. Since the rate of reaction of LOX and gaseous hydrogen is not known, a third simulation was made. The LOX and GOX were assumed to be two separate species, and only the GOX was allowed to react (either to equilibrium or at a finite-rate). The split between LOX and GOX was made along an isotherm somewhat warmer than the critical isotherm, thus, some dense vapor was treated as liquid. Withholding the LOX

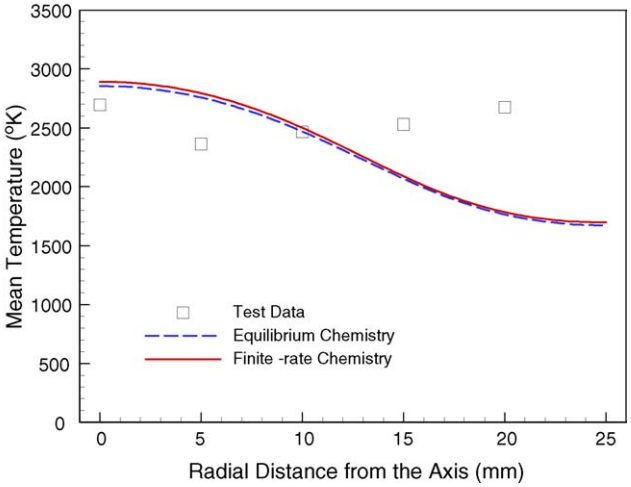

Fig. 8. Comparisons of temperature profile at $X/D = 36$, RCM-2 test case.

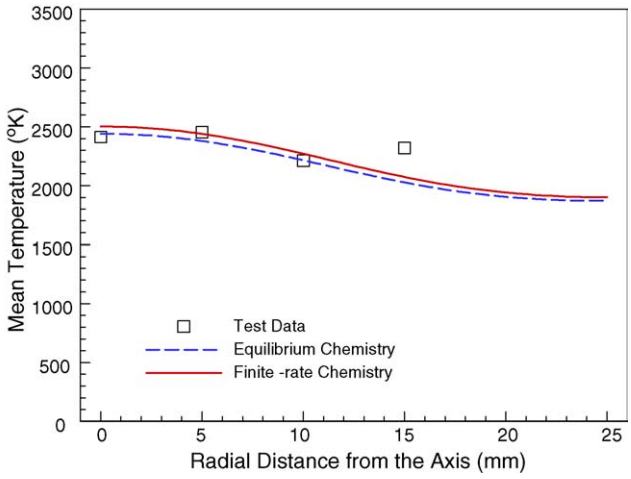

Fig. 9. Comparisons of temperature profile at $X/D = 50$, RCM-2 test case.

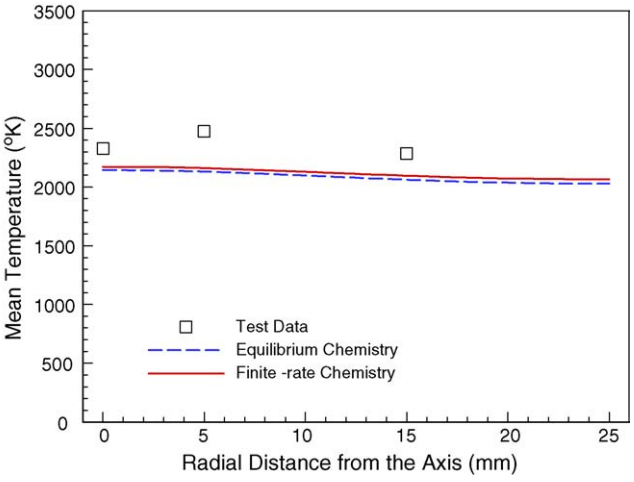

Fig. 10. Comparisons of temperature profile at $X/D = 82$, RCM-2 test case.

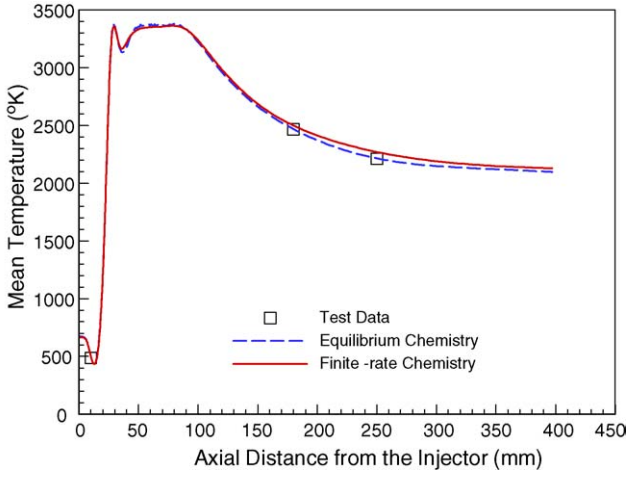

Fig. 11. Comparisons of temperature profile at $R/D = 2$, RCM-2 test case.

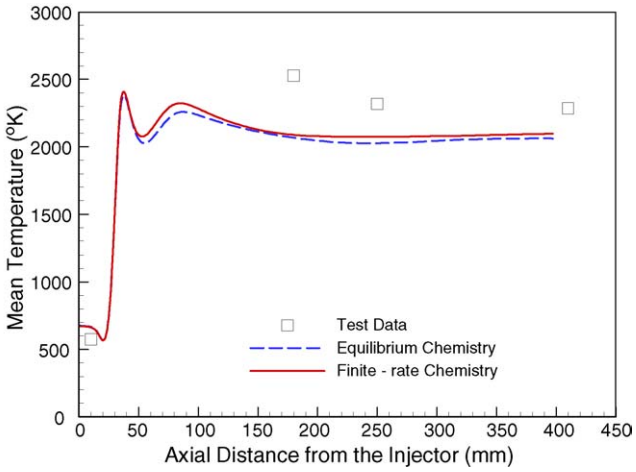

Fig. 12. Comparisons of temperature profile at $R/D = 3$, RCM-2 test case.

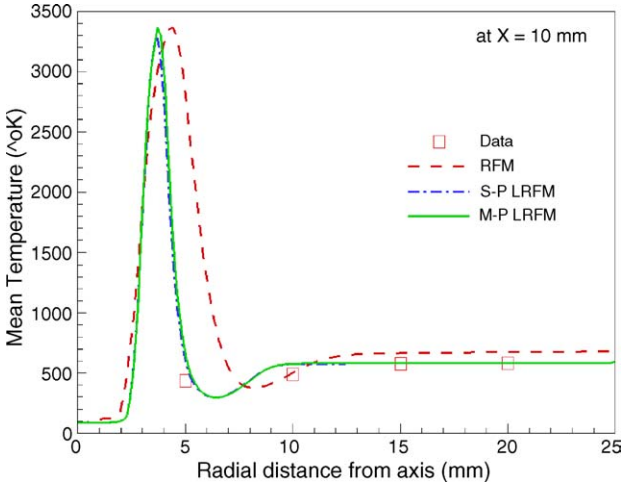

Fig. 13. Effect of omitting LOX reactions.

from the reaction fit the data better near the faceplate, as shown in Fig. 13. The withheld LOX cases fit the downstream profiles differently. The case withholding the LOX from reacting produced thinner shear layers and elongated the flame. The reported measured temperature profiles at $X = 180$ show which appears inconsistent with the other profile data and the simulation. The dip might not be real, but without error bounds on the measurements this cannot be ascertained. At 410 mm, the measurements are bounded by the reaction models. The dramatic effect of the two-species oxygen model on the flame shape was incidental; the change was made to improve the computational efficiency by justifying the use of the simple ideal gas model for the vast majority of grid points.

The final data shown for this case in Fig. 14 are the optical measurements of OH concentrations shown. The comparison of the magnitudes of these measurements is only qualitative, but the shape of the flame is very accurately predicted for the region near the injector face. The simulation made withholding the LOX from reacting spreads slightly faster, but the measured and simulated spread rates are about the same. This indicates that the initial predicted mixing rates are reasonable. This comparison was also made for the supercritical case with the same conclusions drawn from the exercise. The major difference in the reaction models for reacting the LOX and not doing so results in a longer flame (by about twice) for the slower combustion when the LOX is inert. However, the experimental OH map did not extend far enough downstream to verify the flame length. No temperature data were available for the supercritical case.

The treatment of the spray as a homogeneous fluid with turbulent mixing rates as established from conventional turbulence models seems to be reasonable, but critical validation data are still needed. The differences in measured radial temperature profiles, and those predicted are strongly affected by many factors in the CFD model. Whereas only the reaction model was

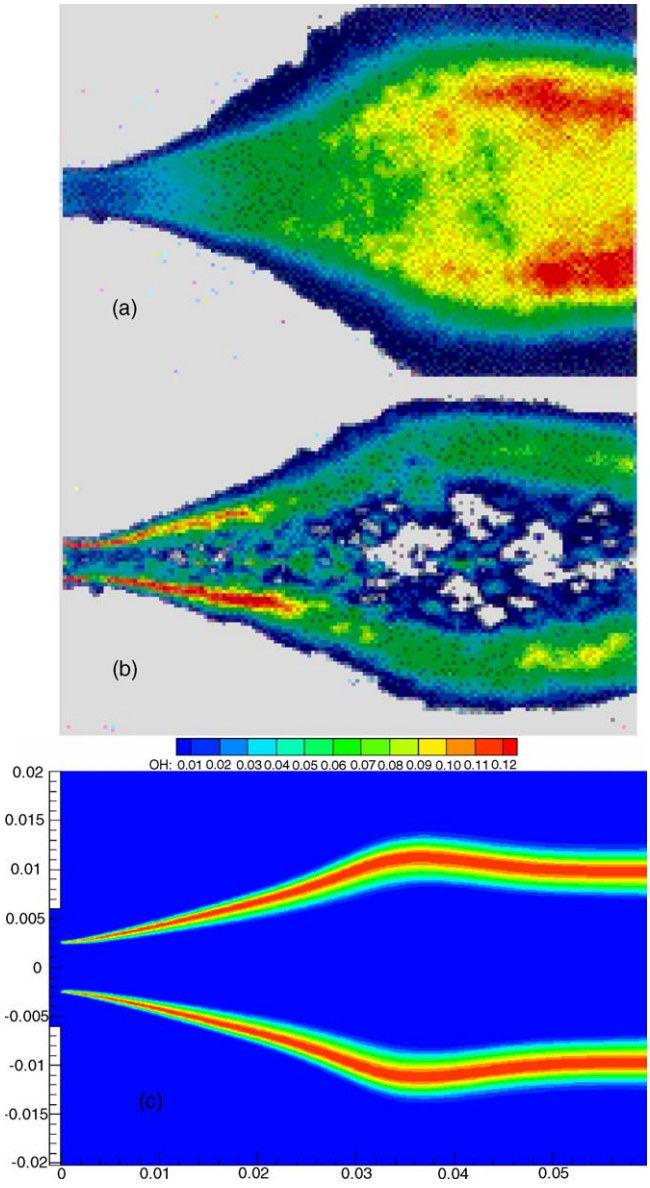

Fig. 14. Comparisons of OH concentrations, RCM-2 test case: (a) time-averaged emission; (b) Abel transformed emission; (c) numerical results.

deliberately changed, density, and turbulent mixing changed as a result. However, without error bounds on the test data further parametric variations in the simulation model would not be worthwhile. Since error bounds are difficult to establish, simple thermocouple measurements along the wall would have provided critical validation data. This is another example of losing valuable information because experiments and analyzes are not performed in concert.

The validation with the IWRCM data proved that simplified engineering analysis applied to the CFD methodology could provide a practical design tool. More validation test data are needed, but no conflicting evidence has been found that the homogeneous spray model is unrealistic. Certainly, the CFD model can be more finely tuned when new test data become available. In the mean time, the new spray combustion model is being used as a design tool to evaluate the efficiency of injector configurations. Others who have tried to model the IWRCM test data with droplet tracking models have encountered great computational inefficiency and have predicted the droplets to dribble down the centerline and not mix as rapidly as the test data indicate. The analyses described herein is the first high-pressure spray flame model that is sufficiently computationally efficient that three-dimensional injector flowfield simulations can be practically made. We cannot yet simulate the injectors with hundreds of elements. But the ability to simulate even a modest number of clustered elements is a significant advance in CFD methodology.

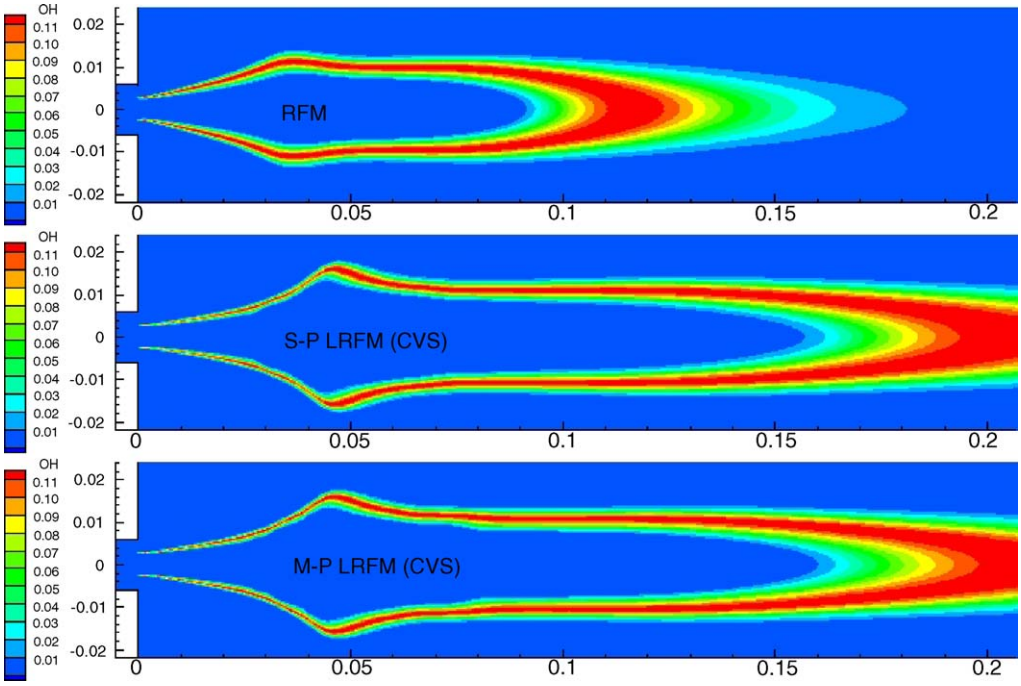

Fig. 15. Comparison of RCM2 jet simulations with and without LOX reactions.

7. Conclusions

(1) A wide variety of processes are represented by very similar sets of PDE conservation laws.
(2) Numerical solutions of these PDE's are practical.
(3) Accepted engineering simplifications to process analyses coupled with CFD methodology greatly increases the range of problems, which can be currently addressed.
(4) Today's CFD simulations are not trusted unless they are "validated." This is the weakness in such methodology. The "validation experiments" are most often not sufficiently similar to the prototype for the verification needed. Also, measurements are insufficient and are not made at critical locations to test the simulation.
(5) Grid generation is not taught to ChE's and Chemists.
(6) Fortran is the established computer language of transport phenomena analysts.
(7) Undergraduate ChE's and Chemists are not exposed to even an elementary CFD code.

8. Recommendations

(1) Practical complex chemical process analysis can be accomplished with CFD simulations, which use two-equation turbulence models and conventional chemical kinetics.
(2) Using CFD methodology without access to the source code is inconvenient and risky.
(3) Establish basic computational transport phenomena code(s) to expedite modeling of complex process analyses by new practitioners.
(4) Include programming, griding, and plotting methodology instruction sufficient to utilize the CTP codes.
(5) Encourage the inclusion of computational transport phenomena methodology in ChE curricula.